# Redetermination of Sensitivity for Grating G140L

L. E. Sherbert, D. R. Soderblom, and J. Mack
May 23, 1997

**ABSTRACT**

*This ISR describes a re-determination of the sensitivity function for grating G140L of the GHRS. This was done after it was determined that the existing functions left significant and systematic residual errors. Definitions of the sensitivity and vignetting functions are provided, and the procedures used to derive them are described and illustrated. Some intrinsic limitations are described of the process of deriving sensitivity for the GHRS and for the ultraviolet in general. New baseline sensitivity functions for G140L, and ones that are time-dependent have now been installed in CDBS.*

## 1. Introduction

When GHRS spectra are calibrated, the observed pixel position is translated to wavelength, and counts are transformed to flux. The calibration of counts to flux depends on wavelength, of course, but otherwise the flux and wavelength transformations are nearly independent of one another. Also, the determination of wavelength relies on a calibration within the instrument (observation of the wavelength calibration lamp), whereas the flux calibration is based on observations of standard stars.

This *Instrument Science Report* is concerned with the determination of the sensitivity function for grating G140L. This grating provides the lowest resolution of any in the GHRS, making the determination of sensitivity both easier and more difficult. It is easier because fewer discrete exposures are needed to cover the full useful range of the grating. It is more difficult because users of G140L data are more likely to need precise and accurate fluxes than users of the higher-dispersion gratings, and small deviations over a spectrum may be difficult to see but can still be important for the interpretation of the results. Also, we now know that the sensitivity of Side 1 of the GHRS is changing with time, especially below Lyman-$\alpha$ (1215 Å).

A significant deviation between a pipeline-calibrated spectrum and expectation led to the investigation that brought about this redetermination. A GO (R. Gilliland) compared reduced G140L spectra to models of white dwarfs and saw systematic differences of several percent that could not be explained. This led him to go back and try to see how observations of a standard star would come out if they were processed as ordinary observations. Those standard star observations showed similar deviations, suggesting that a fundamental problem existed. The deviations seen by Gilliland are shown as the "quick ratio" or x's in Figure 1.

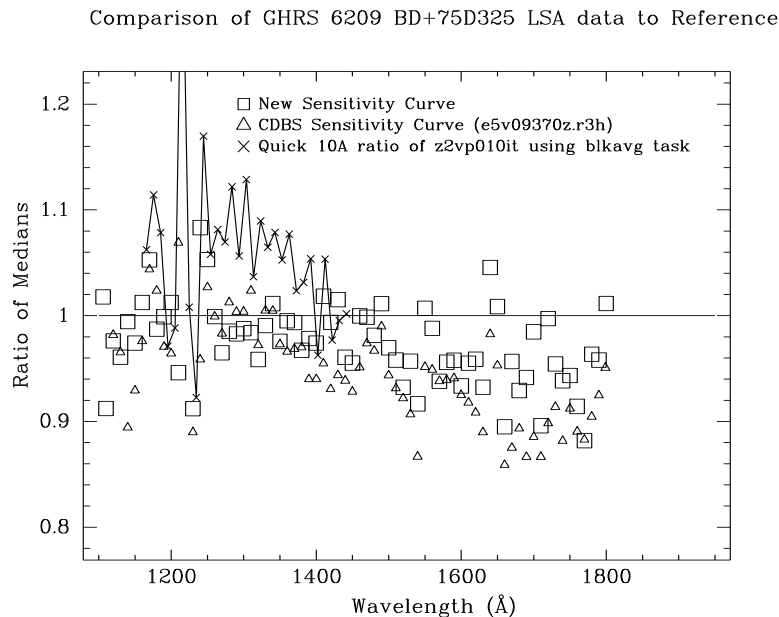Comparison of GHRS 6209 BD+75D325 LSA data to Reference



**Figure 1:** Deviations in the flux calibration of grating G140L. The ratio of the calibrated spectrum to the reference spectrum is shown for the standard star BD+75°325. Also plotted are the CDBS (i.e., pipeline) Sensitivity Curve (triangles) and the new sensitivity curve (square) derived in this paper, all of which are plotted as ratios relative to the previous curves. These new curves are now in CDBS.

We began by confirming that the indicated problem existed in the form identified by the GO. This led us to go back and reread the SER supplied by D. Ebbets when he delivered the G140L sensitivity files in 1994. At that time, G140L – one of the GHRS Side 1 gratings – had just been returned to service after a fix to the GHRS during the First Servicing Mission to *HST*. Also, at that time a fundamental change occurred with regard to ultraviolet flux scales for *HST* in that the white dwarf G191-B2B was used as the fundamental standard. This led to changes of 10 to 20% at some wavelengths in UV flux scales.

The precise source of the problem in the UV fluxes for grating G140L has not been determined, nor do we expect to do so. We suspect it has to do with the change to the white dwarf flux scale and an erroneous application of a correction function, but the prob-

lem does indeed exist and our concern here is with providing an accurate and reliable set of calibration files.

We begin with a short description of the different domains of sensitivity, then describe how the functions were determined.

Also, in this ISR we will use the shorthand "BD+28" for the standard star BD +28° 4211 and "BD+75" for BD +75° 325.

## 2. Sensitivity, Vignetting, and so on

If it were possible to record the full useful wavelength range of a grating in a single exposure, then it would also be possible to determine a single "sensitivity function" for that grating. That function, which we will denote by $S_\lambda$, would have units of flux per count rate[1], or, more physically, $S_\lambda$ is in units of (erg cm$^{-2}$ s$^{-1}$ Å$^{-1}$) per (counts s$^{-1}$ diode$^{-1}$), where knowledge of the instrument's properties indicates the appropriate wavelength at a given diode. We will denote the flux by $F_\lambda$ and the count rate by $C_\lambda$, so that $S_\lambda = F_\lambda/C_\lambda$.

This work would be much easier if we could observe a "perfect" star, by which we mean one with a flat or nearly-flat spectrum which is not variable in time and which is largely free of any structure (such as absorption lines). We also wish we had a "perfect" detector to work with, which would be one with a flat response across its face, that response being independent of wavelength, spatial position, or time.

Real stars, in particular those used as standards for UV flux calibration, have many spectrum features, and those lie at astrophysically-critical wavelengths. The biggest of these, like Lyman-α, are "potholes" in that they must be worked around carefully. There are also weaker features – the "barbs" – that make it difficult to divide one spectrum by another. Real detectors, like those in the GHRS, have response functions that vary with wavelength, and, to some degree, with time. What is particularly difficult to treat is the very steep decline in sensitivity below Lyman-α.

The gratings of the GHRS can be positioned to almost any wavelength within their nominal ranges. When this is done, other effects must be taken into account. In particular, GHRS spectra have a "vignetting" correction applied after the initial sensitivity calibration. This vignetting is only partially so in the classic optical sense, and, in fact, includes several effects that lead to variations in the spectrum of a few percent over scales of tens of pixels. "Sensitivity," on the other hand, is meant to refer to the gross dependence of observed count rate on stellar flux. Thus "sensitivity" should not depend on how a spectrum is placed on the detector; those spatially-dependent effects come under "vignetting." Variations on even finer scales also occur and have to do with diode-to-diode gain variations, granularity, etc. Those small-scale (one to a few diodes in scale) variations will not

---

1. More properly this is the inverse sensitivity. We will ignore the distinction here.

be treated here (but see, for example, GHRS-ISR-076 for a discussion of this "granularity" for G140L).

The underlying concepts used to determine $S$ and separate it from $V$, the vignetting function are simple:

- Observe a standard star over the full useful range of the grating, ensuring that any given wavelength is observed twice by stepping the grating by half its bandwidth. This produces the observed standard star spectrum, in count rate units, $C_\lambda(O)$, as a function of wavelength.

- Plot these overlapping spectra in the units they are observed (count rate) versus wavelength. The central region of each spectrum should form an upper envelope to what is seen.

- Compare this upper envelope to a reference flux spectrum for the standard star, $F_\lambda(R)$. The reference spectrum is the official version of what the flux at each wavelength of the standard star is supposed to be.

- The initial estimate of sensitivity is then $S_1 = F_\lambda(R)/C_\lambda(O)$.

- Use this initial estimate $S_1$ to derive deviations for each individual spectrum. These are $V_1$, determined as a function of position on the detector photocathode, the detector being the presumed source of the variations ascribed to vignetting.

- Iterate $S$ and $V$ until satisfactory closure occurs, to get $S_{final}$ and $V_{final}$. The goal was to determine vignetting to within about 1%.

In practice, of course, determining $S_\lambda$ and $V_\lambda$ is not so simple, and involves some guesses and estimates and compromises. For example, we accepted the existing CDBS G140L vignetting files as final versions and did not attempt to rederive the vignetting: the residuals in overlapping areas of the spectra were within acceptable limits.

Figure 2 shows the first step in this process. The upper frame shows the observed spectrum, $C_\lambda(O)$, of standard star BD+28 in units of count rate, while the bottom frame shows the reference spectrum, $F_\lambda(R)$. Please note that this reference spectrum already takes into account the proper white dwarf flux scale, and that no secondary correction is needed.

## 3. Problems and Limitations

The procedure outlined above leads to reasonably satisfactory results quickly. There remain, however, nagging problems that can be difficult to treat.

### *Far-UV Reference Fluxes*

First, starting with a good reference spectrum involves putting together some pieces. The existing reference spectra of our two standard stars, BD+28 and BD+75, are based on FOS observations, and are on the fundamental UV scale of G191-B2B. However, the GHRS can observe further into the UV than can the FOS, which means that we lack a ref-
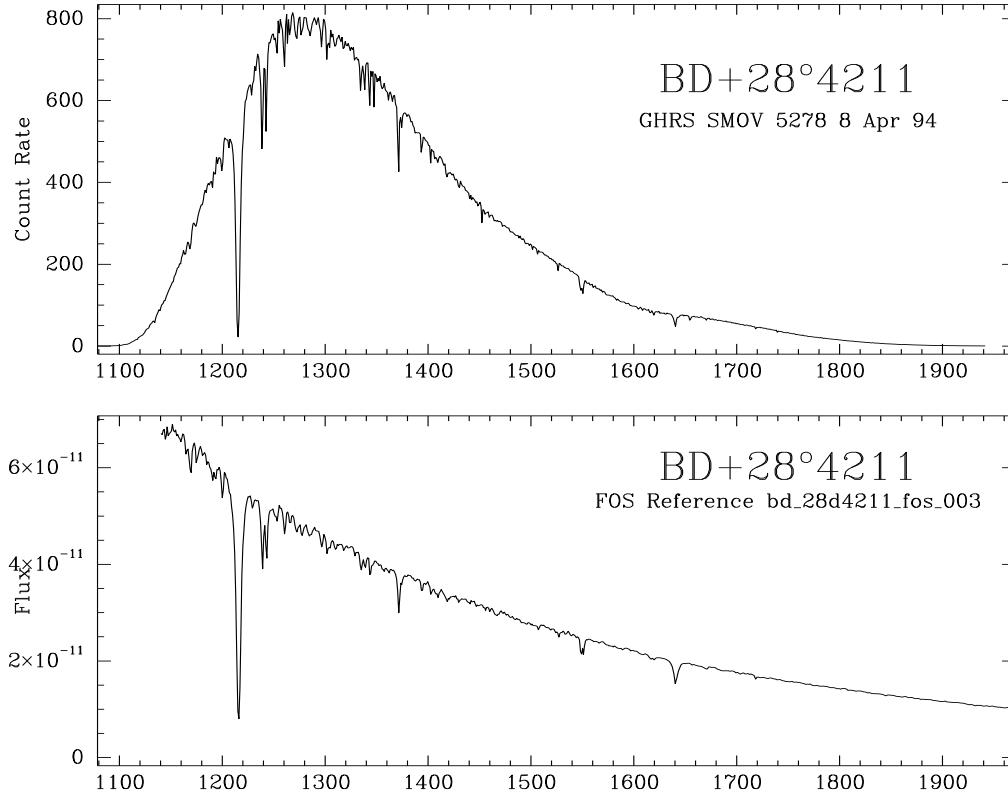
**Figure 2:** Observed spectra $C_\lambda(O)$ of standard star BD+28, compared to the reference spectrum $F_\lambda(R)$ for this star.

erence spectrum below about 1140 Å. Thus we added a HUT spectrum to the FOS reference spectrum for BD+75. The HUT spectrum matches that of the FOS in slope, but not in flux where they overlap. To force them to match we multiplied the HUT spectrum by 1.08. Unfortunately, we have no such data for BD+28.

### Lyman-$\alpha$ and Other Major Features

It is difficult to determine the calibration in the region of Lyman-$\alpha$ because it is such a large feature. Also, Lyman-$\alpha$ lies on a portion of the observed spectrum with a steep slope (Fig. 2). Lyman-$\alpha$ is very broad, and, moreover, there is little spectrum left shortward of Lyman-$\alpha$, and the sensitivity there is declining rapidly. As a result the intrinsic uncertainty in fluxes in the region of Lyman-$\alpha$ is higher than at other wavelengths.

Various features show up in all parts of the spectrum of the standard star, but they are moderate in effect, making it possible to form a reliable estimate of the spectrum. Recall that the reference spectrum is defined in terms of the total stellar flux within some bandpass, meaning that it is *not* the flux in the continuum. The reference spectrum has its origins in FOS observations, at resolution lower than those of the GHRS. Therefore we interpolate both spectra to get the resolution of the GHRS spectra to a level similar to that of the reference spectrum.

### *Small Science Aperture (SSA)*

The amount of light seen through the Small Science Aperture (SSA) is sensitive to the centering of the object in the SSA. The baseline SSA sensitivity curve was created by multiplying the baseline LSA sensitivity curve by the SSA/LSA ratio. The process used is discussed in greater detail later in this document.

### *The Effects of Time*

Ratios of our regular sensitivity monitoring data to the baseline SMOV data show changes in GHRS Side 1 sensitivity over time since the installation of COSTAR,. Each time the monitor was run, the current data was compared to the SMOV BD+28D4211 data at the same wavelength. A ratio and errors were calculated every 10 Å from ~1100 Å to ~1630 Å. While the sensitivity below Lyman-$\alpha$ decreased, an apparent increase occurred in sensitivity from ~1200 to 1350 Å, before it declined again. We do not understand this behavior, but it has remained fairly constant with time.

In addition to rederiving the baseline post-COSTAR sensitivity, we have also created time-dependent curves for the date of each sensitivity monitor based on the ratio of the counts from the monitor to the SMOV baseline data. GOs will need to interpolate between sensitivity curves to get a correction appropriate for the date of their observations.

## 4. The Calibration of G140L

The procedure used was to calibrate the data with calibration switches set as follows:

**Table 1: Calibration Switch Settings**

| SWITCH | SETTING | SWITCH | SETTING | SWITCH | SETTING |
|--------|---------|--------|---------|--------|---------|
| DQI_CORR | PERFORM | VIG_CORR | PERFORM | BCK_CORR | OMIT |
| EXP_CORR | PERFORM | MER_CORR | PERFORM | IAC_CORR | PERFORM |
| DIO_CORR | PERFORM | ADC_CORR | PERFORM | ECH_CORR | OMIT |
| PPC_CORR | PERFORM | MDF_CORR | OMIT | FLX_CORR | OMIT |
| MAP_CORR | PERFORM | MNF_CORR | OMIT | HEL_CORR | PERFORM |
| DOP_CORR | OMIT | BMD_CORR | OMIT | VAC_CORR | OMIT |
| PHC_CORR | PERFORM | PLY_CORR | PERFORM | GWC_CORR | PERFORM |

We used the existing IDT-derived vignetting curves (ebe1353qz.r2h) since residuals derived from comparing overlapping regions are well within acceptable limits.

The data were flat-fielded using the optional G140L LSA flat-fields available in CDBS (ga41342hz.r1h). (The two multi-group flats in CDBS have a problem with the first and last points being INDEF, which leads to a value of zero for the first and last pixels of the

calibrated data. This effect, however, is too small to be of consequence and has been ignored.)

No background subtraction was performed because 1) doing so introduces negative flux values, and 2) the background is low enough that it does not significantly contribute to the flux.

The next major step after calibration is merging the data from the different carrousel positions into one spectrum with the STSDAS task z_calib.mergecar. Using this task, the GHRS data are binned into linear 1 Å wavelength bins, and overlapping areas are averaged together. This binned, merged data can then be divided by the reference spectrum using the STSDAS task z_calib.abssenz (matching wavelength bins), and the result is smoothed to create an absolute sensitivity file. Our reference star data came from the CDBS files bd_28d4211_fos_003.tab and bd_75d325_fos_003.tab (supplemented with HUT data as discussed earlier).

The sensitivity was actually derived several times, using the SMOV program 5278 BD+28 observations, and the BD+75 FP-SPLIT observations from the flat-fielding calibration program 6209, taken in Cycle 5. When deriving a sensitivity curve for the BD+28 data alone, however, we find significant differences from that derived from BD+75. We first thought a sensitivity curve derived from both stars would be best if the curves could be brought into closer agreement. R.Gilliland hypothesized that some of the differences between the two curves could be accounted for by errors introduced by wavelength offsets between the GHRS data and the reference data. We therefore measured the positions of as many lines as possible in the BD+75 and BD+28 data sets corresponding to the reference data, using the task splot. The difference in resolution limited the number of lines in common, but the FP-SPLIT nature of the BD+75 observations gave a large amount of data. No pattern, either in size or in direction, was found describing the differences in wavelength between the reference and the GHRS data. Therefore, an average of all the BD+28 shifts (0.400Å for the LSA, 0.505Å for the SSA) was applied to the merged 5278 GHRS data, and an average of the BD+75 shifts (0.506Å, LSA and SSA) was applied to the merged 6209 data.

Since the BD+75 data (program 6209) were taken over a year after SMOV (22 September 1995), it suffers from the flux changes we have seen in our monitoring program. A flux correction was therefore applied to this data to bring it to the SMOV flux-level. We fit a cubic spline to the ratios derived from the sensitivity monitoring calibration data taken on 17 Sep 95 and divided the BD+75 data by the result.

Two versions of an absolute sensitivity file were created, one based on the GHRS BD+28 data alone, the other a combination of the BD+75 absolute sensitivity and the BD+28 absolute sensitivity. The STSDAS fitting task gfit was then used to fit each dataset with a cubic spline. Two iterations and rejection of 2 sigma were used. Order 20

was decided to be the best because, even though it did not fit the blue end as well, order 50 introduced non-physical bumps and wiggles that order 20 did not.

The fit to the absolute sensitivity calculation is used to create absolute sensitivity and absolute flux wavelength net header files. To test how good the calculation is, the 5278 and 6209 data were flux calibrated using each of the new sensitivity files, and then ratioed in 10 Å bins to the reference data. In a perfect world, these ratios would be flat, but we found the 5278 data calibrated best with the sensitivity based on BD+28 alone, so we chose that version as the new G140L sensitivity. We still have some residuals which we can use as an estimate of the error in the flux calibration. We can also compare these ratios to ones similarly derived from data using the existing G140L LSA calibration, showing that the residuals have decreased overall (see Figures 1 and 3).

In any fitting procedure, the end portions of the data set are fit the worst, if only because the fitting functions have nothing to limit them beyond the scope of the fitted data. One reason for preferring spline function fits was that they are better behaved in this regard, compared to Legendre functions. For the GHRS, the end effects are compounded by the low count levels due to decreased sensitivity in these regions. On the other hand, the practical need for highly accurate fluxes at these wavelengths is less because G140L is not very useful at those points. In other words, we did the best we could to derive satisfactory results, but the consequences of minor errors are not significant.

Since the fit is not as good at the bluest wavelengths (values dropping to negative numbers) and since GHRS essentially has no response below 1100 Å, the data below 1100 Å are forced to curve gently toward a constant value ~ $2.0 \times 10^9$. We need the sensitivity curve to go down to 1040 Å because some GHRS observations extend that far even though there is no signal.

### Data sets used

Although it was observed at fewer grating settings than BD+75, ultimately, we used only the observations of the ultraviolet standard star BD+28 from SMOV program 5278 to derive the new sensitivity for the reasons discussed below. All the data were taken with the standard step pattern (5) and comb addition (four). The observations are listed in Table 2.

The BD+75 observations were not used for several reasons:

- Many absorption lines make the data difficult to work with;
- The merging of the FP-SPLITS was done on the basis of wavelength rather than the alignment of features, which may also have contributed to the noise;
- The changes in GHRS sensitivity make the BD+75 fluxes uncertain;
- The BD+28 continuum is more easily defined, since there aren't as many lines;
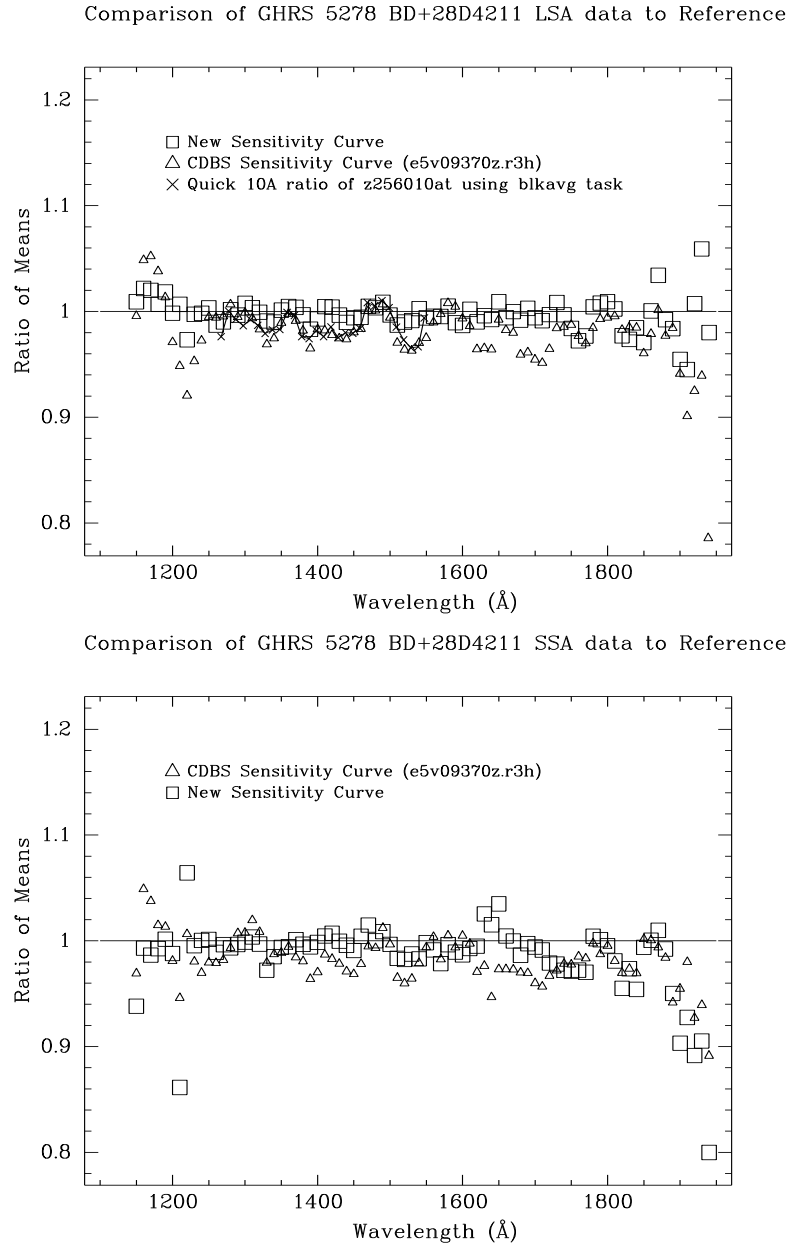- FOS did not observe BD+75 as often as BD+28;

Comparison of GHRS 5278 BD+28D4211 LSA data to Reference



Comparison of GHRS 5278 BD+28D4211 SSA data to Reference



**Figure 3:** Deviations in the LSA (top) and SSA (bottom) flux calibration of grating G140L. The ratio of the calibrated spectrum to the reference spectrum is shown for the standard star BD+28.

- The ratios of BD+75 below 1140 Å gives us doubts about the addition of the HUT data (This only affects wavelengths < 1140Å, and without this data we have to force the curve anyway);

- The BD+75 SSA data in Figure 4 give a ratio lower than 1. This indicates either poor sensitivity for the non-BD+28 SSA data or that the star may not have been centered in the aperture.
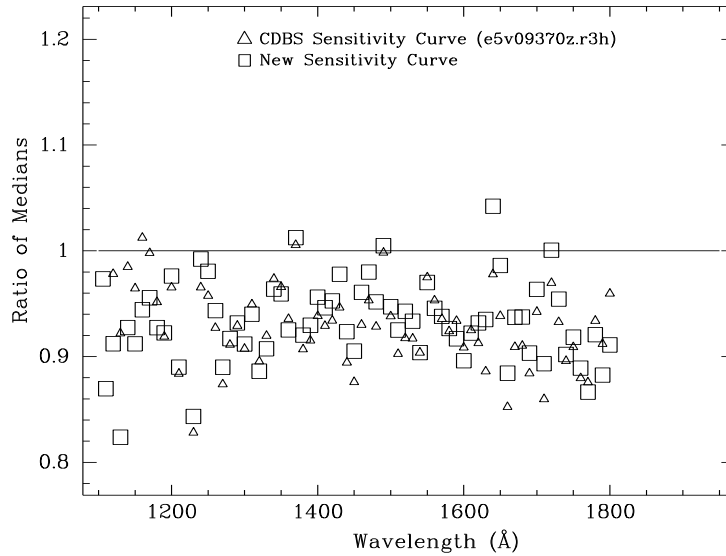
**Figure 4:** Deviations in the SSA flux calibration of grating G140L. The ratio of the calibrated spectrum to the reference spectrum is shown for the standard star BD+75.

**Table 2: Observations of BD+28˚4211**

| ROOTNAME | APERTURE | TARGNAME | EXPTIME (sec) | DATE-OBS | Central Wavelength |
|----------|----------|----------|---------------|----------|--------------------|
| Z2560109T | LSA | BD28D4211 | 27.2 | 08/04/94 | 1203.916 |
| Z256010AT | LSA | BD28D4211 | 27.2 | 08/04/94 | 1406.379 |
| Z256010BT | LSA | BD28D4211 | 54.4 | 08/04/94 | 1596.098 |
| Z256010CT | LSA | BD28D4211 | 272. | 08/04/94 | 1798.361 |
| Z256010GT | SSA | BD28D4211 | 27.2 | 08/04/94 | 1203.986 |
| Z256010HT | SSA | BD28D4211 | 27.2 | 08/04/94 | 1406.451 |
| Z256010IT | SSA | BD28D4211 | 54.4 | 08/04/94 | 1596.17 |
| Z256010JT | SSA | BD28D4211 | 272. | 08/04/94 | 1798.433 |

### SSA and Time Effects

SSA sensitivity was determined by multiplying the LSA curve by the SSA/LSA ratio. In the same manner as the LSA, the SSA data were merged and binned by 10Å with the task `ttools.tstat`, selecting the median over the mean since this is less sensitive to noise. The bins were ratioed and the results fit. The LSA curve was then multiplied by the fit to generate the SSA curve.
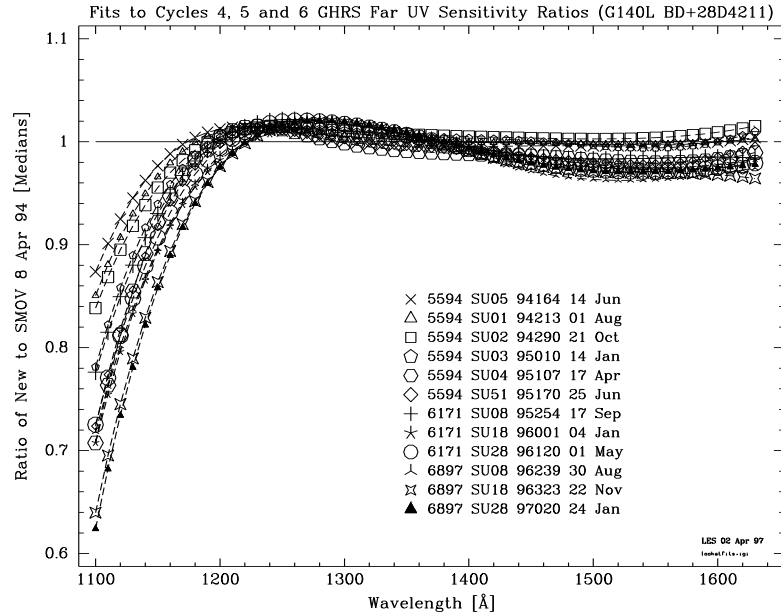
Fits to Cycles 4, 5 and 6 GHRS Far UV Sensitivity Ratios (G140L BD+28D4211)



| | | | | |
|---|---|---|---|---|
| ✕ | 5594 | SU05 | 94164 | 14 Jun |
| △ | 5594 | SU01 | 94213 | 01 Aug |
| □ | 5594 | SU02 | 94290 | 21 Oct |
| ⬠ | 5594 | SU03 | 95010 | 14 Jan |
| ○ | 5594 | SU04 | 95107 | 17 Apr |
| ◇ | 5594 | SU51 | 95170 | 25 Jun |
| + | 6171 | SU08 | 95254 | 17 Sep |
| ★ | 6171 | SU18 | 96001 | 04 Jan |
| ○ | 6171 | SU28 | 96120 | 01 May |
| ⊥ | 6897 | SU08 | 96239 | 30 Aug |
| ⋈ | 6897 | SU18 | 96323 | 22 Nov |
| ▲ | 6897 | SU28 | 97020 | 24 Jan |

LES 02 Apr 97

**Figure 5:**     Fits to the Sensitivity Monitor ratios. Illustrated are cubic-spline fits to the ratios of an observed spectrum to the one observed at the time of SMOV. These fits are the basis for the time-variable G140L sensitivity files.

Ratios of our regular sensitivity monitoring data to the SMOV data show changes in GHRS sensitivity over time since the installation of COSTAR. Since the monitors were centered at 1200Å and 1500Å, but the SMOV data was done at 1200 Å, 1400 Å, 1600 Å, and 1800 Å, there were originally separate ratios for the 1200 Å data and the 1500 Å data, with different baselines. Having different baselines makes it difficult to correct the entire sensitivity curve at once. Therefore, we merged the SMOV data, as well as each of the sensitivity monitoring pairs, and did ratios for each execution of the sensitivity monitor in matching 10 Å bins, covering the range 1100 Å to 1630 Å. These ratios were then fitted with cubic splines of order 3 doing no rejection. Again, we had the option of choosing mean or median values. Since the median is less sensitive to outlying points and because we had decided to ratio median values for the Side 2 sensitivity data, we based the corrections on fits to ratios of the median values, which give slightly steeper slopes at the blue end than do the means. The LSA and SSA sensitivity curves were subsequently multiplied by the fits, illustrated in Figure 5, to create the time-variable sensitivity files.

As we mentioned, we can only correct for time over a limited range of wavelengths because we only observed 2 central wavelengths in the monitoring program. We can only provide time variable sensitivity for 1100 Å to 1630 Å, and in reality we lose a few Ångstroms off those edges due to the way `calhrs` interpolates the sensitivity file. Wavelengths above 1630 Å have been estimated by ratioing the wavelengths where we have data to the baseline, multiplying the baseline by the ratio at the red end, and appending the result to the red end of the time-variable files. A similar process was used for the
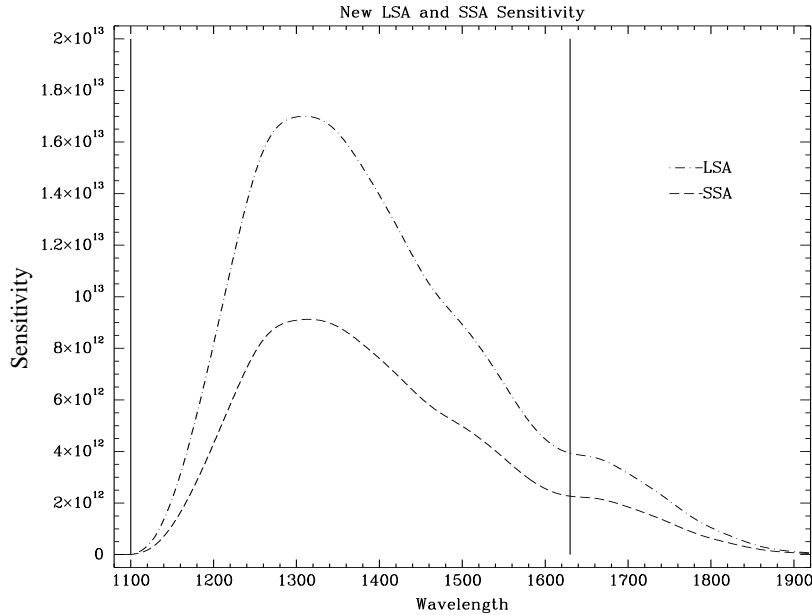
**Figure 6:** New baseline sensitivities for the LSA and SSA. The vertical lines show the wavelength limits (1100Å to 1630Å) of the time-variable sensitivity files. Outside this range, the time-variable sensitivity files are extrapolations.

blue end. The result produces a smooth curve giving complete coverage of the G140L wavelengths.

## 5. Consistency checks

Several checks were performed to ensure that the derived $S$ and $V$ functions are satisfactory. First, we took observed spectra of the standard star BD+28 and calibrated them with this new $S$ function, then compared the results to the reference spectrum of BD+28. The results were presented in Figure 3 for both the LSA and SSA, and show only small residuals.

The same procedure was employed for the BD+75 data from 6209 (see squares in Figures 1 and 4). Since 6209 data was taken many months after SMOV, the BD+75 data first had to be corrected for flux changes on Side 1. A fit to the sensitivity monitoring data on 17 Sep 95 was used for this correction since 6209 executed very closely in time to that monitor. The BD+75 SSA ratio, discussed in Figure 4, is lower than 1, indicating that either the SSA sensitivity file is very poor for non-BD+28 data or that the star was not centered in the SSA.

Third, after creating the time-variable sensitivity files, most of the sensitivity monitor data were flux calibrated using the appropriate file and then divided by the reference spectrum. The same procedure was used on data flux calibrated with the original post-COSTAR G140L sensitivity file (e5v09370z.r3h). Ratios of the newly calibrated data to the reference star are much flatter than the previous ratios (Figure 7).
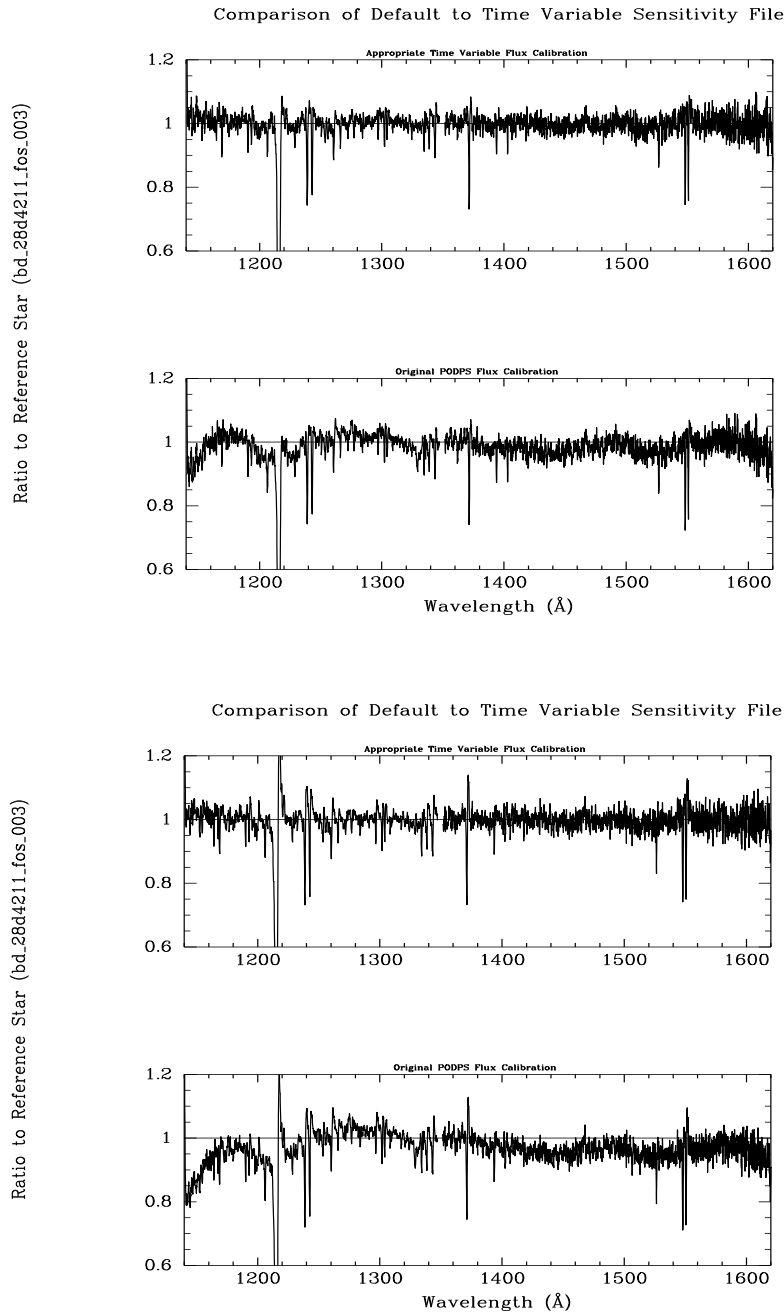
**Figure 7:**     Ratio of Monitor data to reference star. The top plot in each set is flux-corrected with appropriate Time Variable sensitivity file; the bottom plot in each set is the same data calibrated by the pipeline (PODPS). The top set of figures is from Jan 1995 and the bottom set from Jan 1997.

## 6. Conclusion

We have redetermined sensitivity files for GHRS grating G140L and have confirmed that the original vignetting files are satisfactory. Moreover, the changing sensitivity with time of grating G140L, especially below Lyman-$\alpha$, is now provided for through explicit files in CDBS. These new calibration files lead to small residuals that appear to be free of systematic error (Figure 7). Users should note that the baseline sensitivity function (the one determined for immediately after SMOV) validly covers the entire useful wavelength range of G140L, but that the files for later times are only estimated for $\lambda > 1630$ Å and $\lambda < 1100$ Å.